USGS
science for a changing world

Prepared in cooperation with the Air Force Civil Engineer Center

Preliminary Surficial Geologic Map of Leuhman Ridge and the Surrounding Area, Edwards Air Force Base and Air Force Research Laboratory, Kern and San Bernardino Counties, California

By Andrew J. Cyr and David M. Miller

Pamphlet to accompany
Open-File Report 2023–1014

2023

U.S. Department of the Interior
U.S. Geological Survey

U.S. Geological Survey, Reston, Virginia: 2023

For more information on the USGS—the Federal source for science about the Earth, its natural and living resources, natural hazards, and the environment—visit https://www.usgs.gov or call 1–888–ASK–USGS.

For an overview of USGS information products, including maps, imagery, and publications, visit https://store.usgs.gov.

Suggested citation:
Cyr, A.J., and Miller, D.M., 2023, Preliminary surficial geologic map of Leuhman Ridge and the surrounding area, Edwards Air Force Base and Air Force Research Laboratory, Kern and San Bernardino Counties, California: U.S. Geological Survey Open-File Report 2023–1014, 1 sheet, scale 1:18,000, pamphlet 15 p., https://doi.org/10.3133/ofr20231014.

Associated data for this publication:
Cyr, A.J., and Miller, D.M., 2023, Digital database for the preliminary surficial geologic map of Leuhman Ridge and the surrounding area, Edwards Air Force Base and Air Force Research Laboratory, Kern and San Bernardino Counties, California: U.S. Geological Survey data release, https://doi.org/10.5066/P9WTKPBP.

Mahan, S.A., Gray, H.J., Cyr, A.J., Krolczyk, E.T., and Miller, D.M., 2021, Data release for luminescence—Edwards Air Force Base (CA) and CA Water Science Center report including luminescence data and ages: U.S. Geological Survey data release, https://doi.org/10.5066/P9IXG2JX.

ISSN 2331-1258 (online)

Acknowledgments

This geologic mapping is a product of a cooperative study between the U.S. Geological Survey National Cooperative Geologic Mapping Program supported Western Basin and Range—Eastern California Shear Zone geologic mapping project, the U.S. Geological Survey (USGS) California Water Science Center, and the United States Air Force Civil Engineer Center. We thank Allen Christensen and Nicole Fenton (USGS), and Nicholas Teague (formerly USGS, now City of San Luis Obispo Water Resources), who provided data and knowledge from previous work in the Air Force Research Laboratory (AFRL). We also thank Peter Robles, BB&E Consulting, for facilitating access to the AFRL and Edwards Air Force Base. Luminescence analyses and interpretations were conducted by Shannon Mahan, Harrison Gray, and Emma Krolczyk (USGS), without whom the map would have no quantitative geochronologic control. Discussions with Victoria Langenheim and Rufus Catchings (USGS) about geophysical data and shallow seismic data, respectively, of the area improved fault locations. We also thank Lee Amoroso (USGS) for sharing notes from earlier reconnaissance mapping in parts of the current map area, Geoffrey Cromwell (USGS) for details of the well log records for the AFRL, and Geof Spaulding (CH2M Hill [now Jacobs Engineering]–Emeritus and Terra Antiqua) for helpful discussion of hydrologic aspects of this report. Both the map and text of this report benefitted from thoughtful, constructive reviews by Scott Bennett and Ben Melosh (USGS). Rebecca Lambert and Linda Woolfenden (USGS) provided helpful comments that improved the "Hydrologic Implications" section. Regan Austin provided a helpful and thorough editorial review.

Contents

Figures

Table

Conversion Factors

International System of Units to U.S. customary units

Multiply	By	To obtain
	Length	
centimeter (cm)	0.3937	inch (in.)
millimeter (mm)	0.03937	inch (in.)
meter (m)	3.281	foot (ft)
kilometer (km)	0.6214	mile (mi)
kilometer (km)	0.5400	mile, nautical (nmi)
meter (m)	1.094	yard (yd)

Datum

Vertical coordinate information is referenced to the North American Vertical Datum of 1988 (NAVD88).

Horizontal coordinate information is referenced to the North American Datum of 1983, UTM Zone 11 (NAD83 11N).

Abbreviations

AFRL	Air Force Research Laboratory
$CaCO_3$	calcium carbonate
CAM	central age model
CI	color index (percent of dark minerals in a rock)
D_R	dose rate
EAFB	Edwards Air Force Base
ECSZ	Eastern California Shear Zone
Ge	germanium
GIS	geographic information system
ICP-MS	Inductively coupled plasma-mass spectrometry
K	potassium
ka	kilo annum, or thousands of years ago
Ma	mega annum, or millions of years ago
pIR–IRSL	post-infrared–infrared stimulated luminescence
ppm	parts per million
Th	thorium
U	uranium
USGS	U.S. Geological Survey

Preliminary Surficial Geologic Map of Leuhman Ridge and the Surrounding Area, Edwards Air Force Base and Air Force Research Laboratory, Kern and San Bernardino Counties, California

By Andrew J. Cyr and David M. Miller

Abstract

This preliminary geologic map presents mapping of the Leuhman Ridge area of Edwards Air Force Base, California, conducted between April 2020 and June 2021. The report focuses on surficial materials and bedrock to evaluate potential faults and other geologic features that may influence groundwater movement. The preliminary work confirms that the Spring Fault, previously mapped by Dibblee (1960, 1967), is a Quaternary-active fault but does not find convincing evidence to support the existence of the Leuhman Fault (Dibblee, 1960; 1967) within the map area. Several more possible and probable faults are identified by a combination of geomorphic lineaments and brecciated rock. Pleistocene and Holocene eolian deposits are widespread, manifesting as sand sheets, dunes, and admixtures into alluvial fans. Also, an incised pediment forms much of the upland south of Leuhman Ridge. In general, field observations indicate that Quaternary alluvial and eolian deposits are thin; this suggests that secondary bedrock porosity and permeability, defined by degree of weathering and fracture density that includes fault-related fracturing, are more important factors in the location and flow patterns of groundwater.

Introduction

Communities and military installations in the arid Mojave Desert depend on groundwater for their water supplies. Faults can act as conduits or impediments to groundwater flow because of their effects on the physical properties of the geologic materials that they cut (for example, Caine and others, 1996). To improve our understanding of fault controls on groundwater movement in the Air Force Research Laboratory (AFRL) area of Edwards Air Force Base (EAFB) we conducted geologic mapping of surficial deposits and bedrock to refine the locations and characteristics of the previously mapped Leuhman and Spring Fault Zones.

The AFRL is located in the northern Antelope Valley, a generally low relief, internally drained basin between the Transverse Ranges on the south and the southern Sierra Nevada on the north (fig. 1). Topography in the AFRL is dominated by the northeast-trending, linear Leuhman Ridge (fig. 2); the western piedmont of Leuhman Ridge slopes down to the west and the eastern piedmont slopes down to the northeast into an alluvial valley between Leuhman Ridge and an adjacent pediment on the west and south, and the Kramer Hills on the north (fig. 2).

Geologic Setting

EAFB and the AFRL are located in the generally low-relief western Mojave Desert, characterized by Cenozoic sedimentary basins separated by low hills underlain by Mesozoic granitic and metasedimentary rocks and Tertiary volcanic rocks (Dibblee, 1960; 1967). The lowest parts of the western Mojave, west of Leuhman Ridge, are occupied by dry lakes or playas. These provide a source of sand and finer grained sediment that comprise common eolian and eolian-affected alluvial deposits. In the AFRL, younger eolian sediments (Qyes, Qyed, Qyae) are likely derived from Rogers Dry Lake bed (fig. 1), whereas older eolian deposits (Qie, Qies, Qiae) were likely derived from dried lake sediments of paleo Lake Thompson (Orme, 2008) that was located in the Rogers Lake basin.

The Spring and Leuhman Faults (Dibblee, 1960), located in the eastern and central part of the map area, are part of the Mojave strike-slip province. The western Mojave Desert is cross-cut by faults of the Mojave strike-slip province (Miller and Yount, 2002), a region of Pleistocene and older deformation between the Garlock and San Andreas Fault Systems to the west and the younger strike-slip and transpressional faults of the Eastern California Shear Zone (ECSZ) to the east (Dokka and Travis, 1990). The Mojave strike-slip province is wider than and encompasses the active ECSZ (Miller and Yount, 2002). It has been active since approximately 10 mega-annum (Ma) (Nuriel and others, 2019).

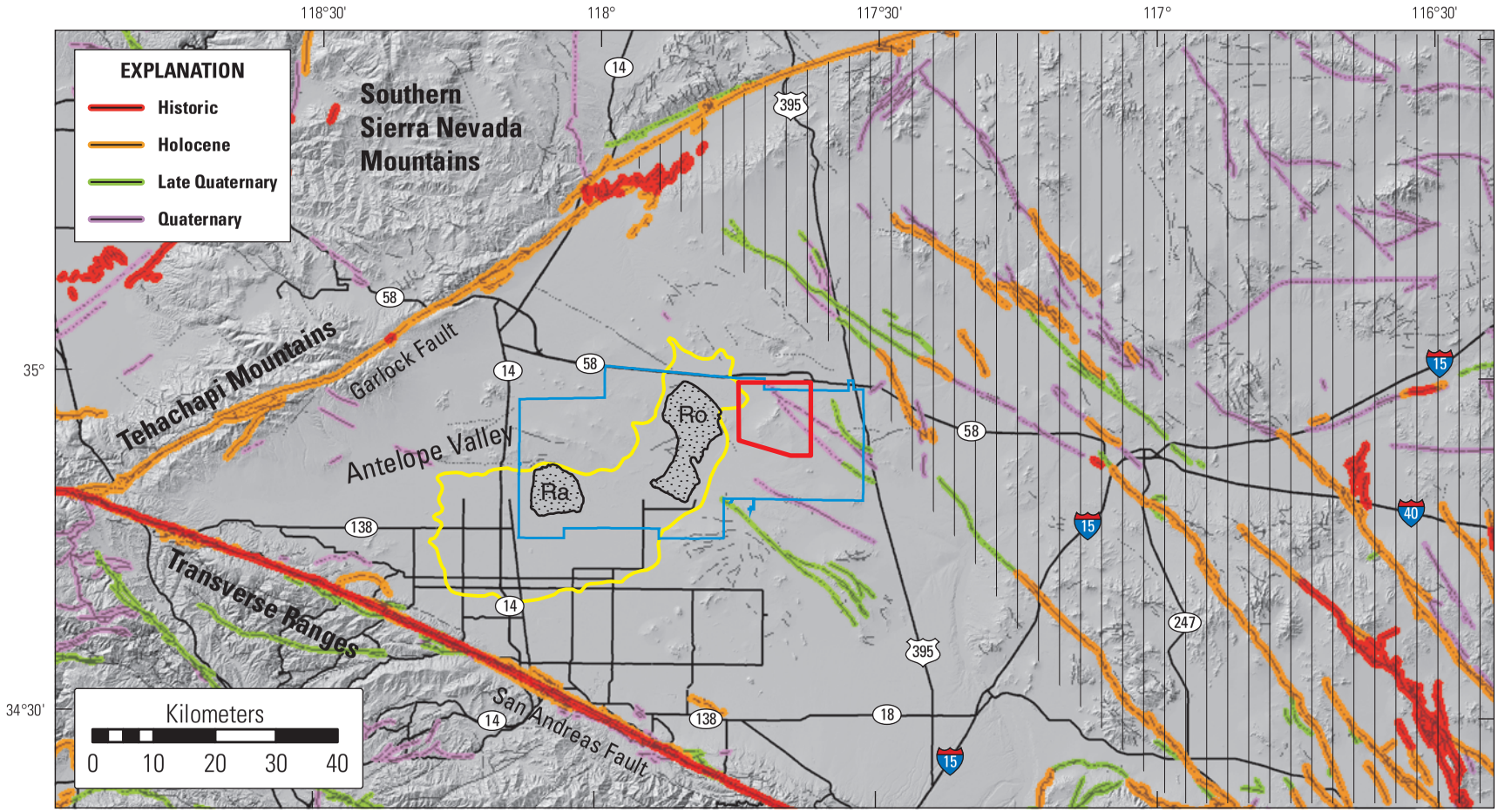

Figure 1. Regional map showing the location of the Leuhman Ridge study area (red polygon) and Edwards Air Force Base (blue polygon) in the western Mojave Desert, southern California. Colored lines show age of known most recent activity on faults in the region (U.S. Geological Survey and California Geological Survey, 2019). Historic, less than 150 years old; Holocene, less than 15 kilo-annum (ka); Late Quaternary, less than 130 ka; Quaternary, less than 1.6 mega-annum (Ma). Major roads and highways shown as black solid lines. Current extent of Rogers (Ro) and Rosamond (Ra) Dry Lakes shown by stippled polygons. Extent of paleo Lake Thompson (Orme, 2008) shown by yellow line. Vertical lines show extent of the Eastern California Shear Zone (ECSZ). Base modified from U.S. Geological Survey National Geospatial Technical Operations Center (2022). Hillshade from U.S. Geological Survey digital elevation model data (U.S. Geological Survey, 2019).

Methods

We used standard geologic mapping techniques to conduct detailed field-based investigations of surficial materials, with an emphasis on the area around Leuhman Ridge and south of the western Kramer Hills (fig. 2; accompanying map sheet). Mapping included digging shallow pits to examine soil profiles and evaluating outcrops and geomorphic features for the presence of youthful faults. Mapping also included study of bedrock, both for clues about offsets on faults and for information on rock properties near and within fault zones. Location control for mapping was by hand-held global positioning system device and tablet computer, with an estimated 5-meter (m) horizontal accuracy. Interpretations of satellite imagery (Maxar Web Map Service accessed in ArcGIS Pro courtesy of the U.S. Geological Survey [USGS]) and 1-m-resolution lidar topography (USGS, 2019) were used to identify subtle geomorphic features that were then investigated in the field. The mapped surficial deposits are classified on the basis of age and depositional process, with age provided in large measure by interpreting soil characteristics and geomorphology of a deposit, similar to the approach outlined in Miller and others (2009). We provide a tabulation of all field stations in the accompanying geographic information system (GIS) database (Cyr and Miller, 2023).

Numeric age control on selected surficial geologic units is based on post-infrared–infrared stimulated luminescence (pIR–IRSL) geochronology. Mineral separation and analysis were completed at the USGS luminescence laboratory at the Denver Federal Center in Lakewood, Colorado. Details about methods, data reduction, and numeric age determination are provided in Mahan and others (2021).

Previous Work

Geologic mapping by Dibblee (1960, 1967) and Ward and Dixon (2002a, b) described the framework bedrock geology of the Leuhman Ridge map area as consisting of Mesozoic plutonic granitic rocks, Tertiary volcanic and sedimentary rocks, and Quaternary alluvial and eolian sediments. Dibblee (1960) also recognized two northwest-striking faults, the Spring and Leuhman Faults, in the northeastern part of the map area (fig. 2). The Spring Fault juxtaposes quartz monzonite (now termed granite) against Quaternary alluvial deposits along the southwestern side of the Kramer Hills. The subparallel Leuhman Fault, between approximately 0.5 and 2 kilometers (km) to the southwest, is inferred beneath Quaternary alluvial and eolian deposits in our map area. This previous work did not study these faults in detail in the area of our mapping.

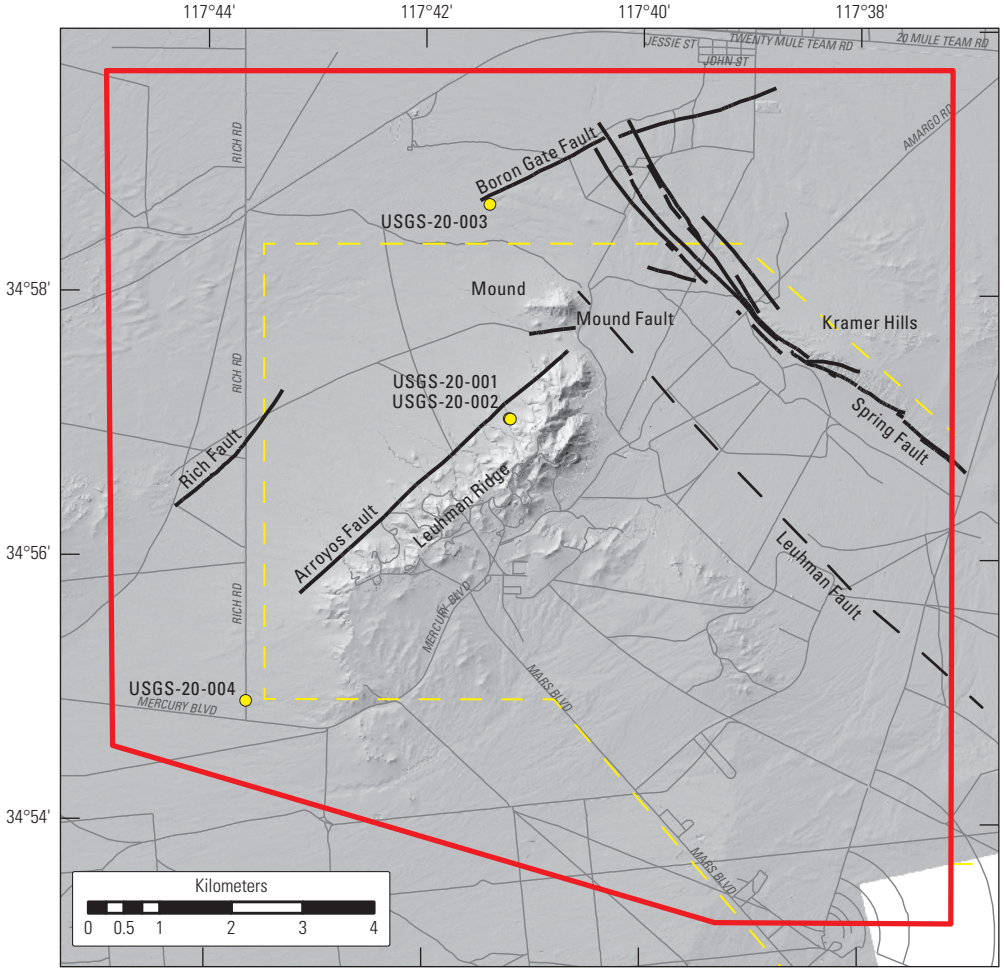

Figure 2. Location map of part of the Air Force Research Laboratory (AFRL), northeast Edwards Air Force Base, California, showing faults described in the text and shown on the geologic map. Red polygon is area of surficial geologic map. Dashed yellow line is approximate boundary of the AFRL. Solid black lines are faults described in this report. Long dashed black line is projected trace of the Leuhman Fault (Dibblee, 1960). Yellow dots are locations with names of samples collected for luminescence geochronology (table 1). Base modified from U.S. Geological Survey, Leuhman Ridge, 2018, scale 1:24,000; and Kramer Junction, 2018, scale 1:24,000. Hillshade from U.S. Geological Survey digital elevation model data (U.S. Geological Survey, 2019).

Detailed gravity surveys to determine the thickness of basin fill deposits (defined as Cenozoic sedimentary and volcanic rocks) have also been conducted at EAFB. Langenheim and others (2019) determined, on the basis of inversion of gravity data combined with geologic map and subsurface well information, that the depth to bedrock around Leuhman Ridge is shallow, generally less than 1 km. Exceptions in the area mapped for this study include local depressions as deep as 1.2 km north and south of Kramer Hills and northwest-trending depressions approximately 4 km northeast of Rogers Dry Lake (fig. 1; Langenheim and others, 2019). Langenheim and others (2019) also observed that neither the Spring nor the Leuhman Faults coincide with large variations in basin fill thickness or prominent gravity gradients. They concluded that this indicates minor vertical and horizontal displacements.

Stratigraphy and Structure

Bedrock and Pediment Surfaces

Bedrock in the map area is composed primarily of Cretaceous(?) granite and granodiorite exposed in the Kramer Hills, Leuhman Ridge, and Mound. Isolated small (less than a few meters high) outcrops of bedrock can also be found in washes along the southern edge of the Kramer Hills and exposed at the bases of arroyos draining the eastern side of Leuhman Ridge (fig. 2). This is consistent with inversions of gravity data (for example, Langenheim and others, 2019) showing that bedrock is relatively shallow beneath a veneer of low-density deposits. Leuhman Ridge is composed primarily of moderately to highly fractured leucocratic granite (Klg), with fracture density increasing near the low pass between Leuhman Ridge and Mound. Mound is composed of leucocratic granite (Klg) and leucocratic granodiorite (Kgdl). Granite (Kg) and granodiorite (Kgd) exposed in the Kramer Hills are unfractured to moderately fractured; the granodiorite weathers to grus.

Bedrock is also exposed in pediments to the south and east of Leuhman Ridge, where it is typically overlain by a veneer of loose alluvial sediment consisting of weathered bedrock (Qpv). These pediments are relatively low relief landforms underlain by unfractured to moderately fractured, commonly deeply weathered, Cretaceous granite (Kg) and granodiorite (Kgd) that weathers to grus.

Quaternary Deposits

Alluvial fan deposits occur primarily on the western piedmont of Leuhman Ridge and in the low-relief valley between the Kramer Hills and the pediment to the south and east of Leuhman Ridge. These deposits can be assigned relative ages using surface characteristics and the degree of soil development. Most alluvial fan deposits in the mapped area include abundant sand and silt derived from windblown materials, which complicates using strict map-unit criteria because the addition of eolian materials modifies both surface and pedogenic characteristics of alluvial fan deposits (Miller and others, 2009). We have designated alluvial fans containing significant amounts of eolian material units Qyae and Qiae. Alluvial fan deposits that do not have significant additions of eolian materials, such as units Qya and Qia, are restricted to the northeastern side of Leuhman Ridge and the easternmost southwest facing piedmont of the Kramer Hills; these locations have either been sheltered from or are longer distances from the sources of eolian materials in Rogers Dry Lake bed and deposits of paleo Lake Thompson.

Eolian sand in the form of sheets and dunes is widespread in the western part of the map area, between the northeastern edge of Rogers Lake and the west and north sides of Leuhman Ridge. Although most of the eolian deposits depicted on the map are young sand sheets (Qyes) and dunes (Qyed), intermediate-age eolian sand-sheet deposits (Qies) are commonly exposed where younger eolian and alluvial fan deposits have been eroded, or in wash cuts and arroyos where the older sand-sheet deposits (Qies) directly overlie Cretaceous granite and are overlain by younger eolian or alluvial fan deposits. These intermediate-age eolian sand-sheet deposits have strong soil characteristics, including strong Bw and Stage III^{+} to IV^{-} pedogenic carbonate development (following Gile and others, 1966; Machette, 1985).

In order to constrain the depositional ages of Quaternary geologic units affected by faults, we collected four samples of eolian and mixed alluvial and eolian deposits for numeric age determination using luminescence methods (see sample location on figure 2; Mahan and others, 2021). Three of these were collected from intermediate-age sand-sheet and mixed alluvial fan and eolian deposits (Qies and Qiae) and one from a young eolian sand-dune deposit (Qyed). Sample USGS-20-003 was collected from a shallow, hand-dug pit. All other samples were collected from exposures either in arroyos or road cuts. Numeric ages are presented in table 1.

In a restricted area east of Mound (fig. 2), intermediate-age groundwater-discharge deposits (Qigw) represent local paleo-wetlands. These deposits consist of poorly to moderately sorted sand- to clay-sized sediment cemented by carbonate that has an irregular "popcorn" texture. Groundwater-discharge deposits appear to interfinger with intermediate-age eolian sand-sheet deposits (Qies) and are overlain by young mixed alluvial and eolian sediments (Qyae). These Quaternary groundwater-discharge-related deposits occur in low-relief depressions between low hills of Cretaceous granitic rocks (Kgb, Kgd, Kgdl), and may correspond with splays of the Spring Fault (see "Spring Fault" section).

Faults

We mapped several faults that cut both Cretaceous and Quaternary units in the map area. Here, we describe the probable age and displacement of principal faults in the map area, with particular focus on faults with evidence of Quaternary activity. One of these faults, the Spring fault, was previously identified and mapped by Dibblee (1960) and appears in the Quaternary fault and fold database (U.S. Geological Survey and California Geological Survey, 2019). We found no surficial geologic evidence of the Leuhman fault, a second previously identified fault also present in the Quaternary fault and fold database (U.S.

Table 1. Luminescence geochronology data, Leuhman Ridge and vicinity, Kern and San Bernardino Counties, California.

[Data from Mahan and others (2021). Ages are post-infrared–infrared stimulated luminescence. No., number; latitude and longitude in decimal degrees north and west; m, meter; %, percent; ppm, parts per million; D_R, dose rate; Gy/ka, gray per kilo-annum; ka, kilo-annum]

Lab no.[1]	Map unit	Latitude	Longitude	Elevation[2] (m)	Depth[3] (m)	Water content[4]	K[5] (%)	U[5] (ppm)	Th[5] (ppm)	D_R[6] (Gy/ka)	Age[7] (ka)
USGS-20-001	Qyae	34.9507	117.6869	873	5.0	3 (22) [3]	2.60±0.05	1.11±0.10	3.93±0.46	3.92±0.15	8.32±0.71
USGS-20-002	Qied	34.9506	117.6869	871	11.1	4 (19) [4]	3.58±0.05	1.32±0.15	4.41±0.46	4.90±0.17	15.2±0.7
USGS-20-003	Qies	34.9778	117.6902	757	1.1	2 (22) [4]	3.13±0.05	2.35±0.15	6.68±0.38	4.91±0.17	25.7±1.2
USGS-20-004	Qiae	34.9154	117.7270	791	1.0	4 (32) [6]	3.50±0.05	2.75±0.15	6.93±0.41	5.28±0.20	38.9±2.9

[1]All samples processed at the U.S. Geological Survey Luminescence Geochronology Lab in Denver, Colo.

[2]Elevation of ground surface.

[3]Depth below ground surface

[4]Percent water content of field sample used for age calculation, number in parentheses is saturated water content, number in square brackets is water content used in age calculation.

[5]Determined by high-resolution Ge gamma ray spectroscopy or inductively coupled plasma-mass spectrometry (ICP-MS).

[6]Environmental dose rate; calculated using the Dose Rate Age Calculator (Durcan and others, 2015).

[7]Central age model (CAM) age in thousands of years; determined using the function calc_CentralDose from the R-Luminescence package (Kreutzer and others, 2012). Uncertainty is 2 σ.

Geological Survey and California Geological Survey, 2019). We used a combination of field mapping and analysis of satellite imagery (Maxar Web Map Service accessed in ArcGIS Pro courtesy of the USGS) and 1-m-resolution lidar topographic data (USGS, 2019) to look for evidence of Quaternary fault rupture, including offset geomorphic features such as wash edges or ridges; fault scarps cutting Quaternary deposits; deformed Quaternary deposits; lithologic changes, changes in lithologic characteristics, such as fracture density; apparent changes in vegetation assemblage; and sharp changes in color. Because older faults also affect groundwater flow, we examined bedrock exposures for pre-Quaternary faults but did not find evidence for older faults that do not also affect Quaternary deposits.

Spring Fault

The Spring Fault, originally identified by Dibblee (1960, 1967), is in the northeastern corner of the map area. It strikes northwest along the southwestern edge of the Kramer Hills, and bends to the north-northwest, where it splays into several subparallel strands (fig. 2). The Spring Fault continues to the southeast, beyond the map area. However, the southern approximately 4 km of the Spring Fault in the map area juxtaposes a short (approximately 0.5-km-wide), southwest-facing piedmont along the Kramer Hills that is formed primarily by young alluvial fan deposits (Qya and Qya4) and mixed alluvial fan and eolian deposits (Qyae and Qyae4). These alluvial fan deposits and the alluvial fraction of the mixed alluvial fan and eolian deposits originated from Cretaceous granodiorite (Kgd) and granite (Kg) to the north and east. Here the fault forms a major linear ridge characterized by multiple scarps in Qya and Qia alluvium and by breccia and gouge where it cuts through Kgd and Kg crystalline bedrock. In other parts of the Mojave Desert, numeric geochronology has constrained the ages of similar Qya4 deposits to between approximately 14 and 9 kilo-annum (ka) (for example, Miller and others, 2009), making the most recent activity on the southeastern part of the Spring Fault latest Pleistocene to Holocene in age.

Along its northern approximately 4-km extent, the Spring Fault splays into a horsetail comprising at least five separate strands that strike between approximately 285° and 330° in a zone that increases in width from approximately 250 to 900 m towards the northwest (fig. 2). The horsetail pattern was identified by field work guided by analysis of lidar topography and expands on the simple single-strand geometry mapped by Dibblee (1960, 1967); the location of the single strand depicted on Dibblee's map does not coincide with any of the five strands identified by our detailed studies. The fault splays bound separate low, northwest-trending linear ridges of Kg crystalline rocks that stand above Holocene and Pleistocene eolian sand-sheet deposits (Qyes and Qies) and Holocene mixed alluvial and eolian deposits (Qyae). The northeastern two splays are likely the primary strands of the Spring Fault, on the basis of their relationship to the Boron Gate Fault (see description in "Boron Gate Fault" section). These are concealed by Quaternary deposits as old as late Pleistocene (Qies), which do not exhibit evidence of fault deformation. However, splays of the Spring Fault do form scarps and small fault-parallel elongated depressions in the granitic rocks. Several of the probable southwestern splays of the Spring Fault, which lie under an active wash deposit (Qaw) cannot be observed to cut any deposits. Southwestern splays of the fault zone lie adjacent to or cut exposures of intermediate-age groundwater-discharge deposits (Qigw). Such cross-cutting relationships indicate that these fault splays may have contributed to ponding of shallow groundwater.

Although the Spring Fault has affected Holocene and older alluvial deposits (Qya and Qia), we did not observe any offset Quaternary features that allow a determination of the amount

of late Quaternary fault slip. However, previous work described evidence of displacement of Cretaceous(?) crystalline bedrock (Kg and Kgd). On the basis of maximum scarp height, Dibblee (1960, 1967) estimated approximately 45 m of relative uplift on the northeastern side of the Spring Fault. A recent gravity model of depth to basement (Langenheim and others, 2019) estimated a slight deepening of the bedrock surface on the western side of the fault, from 0 m (bedrock exposed at the surface) to as deep as 125 m. Both observations are consistent with relative down to the southwest displacement.

The northwestern extent of the Kramer Hills ends in an approximately 072°-trending, low-relief, 5- to 12-m-high scarp that corresponds with the northwest limit of granitic outcrops. We interpret this northwest-facing topographic front as a fault (see "Boron Gate Fault" section), which appears to be right-laterally offset approximately 50 m across two splays of the Spring Fault, indicating that the Spring Fault is the younger of the two structures. The Spring Fault cuts units Kg and Kgd in the Kramer Hills, with unit Kgd adjacent to the fault along much of its length. Northward, unit Kgd is cut out by the fault. We observed that the northernmost narrow wedge of unit Kgd is mainly breccia and highly fractured rock. Because this breccia may be fault rock strung out along the fault and, therefore, not a meaningful indicator of total offset, we ignore this breccia in the following analysis. West of the Spring fault, unit Kgd is intermixed with a leucocratic variant of the unit (Kgdl) and minor gabbro (Kgb). These latter two units are present in the Kramer Hills in and near the granodiorite unit but not in bodies large enough to warrant mapping as a distinct unit. Unit Kg occurs within the eastern splays of the fault but not west of the full set of splays. The absence of Kg southwest of the Spring Fault indicates that the length of fault cutting Kg on the northeast is the minimum amount of total offset on the fault. These relations indicate that greater than 3.5 km of offset has displaced unit Kgd and its related subunits across the fault zone. About 1.7 to 2.2 km of minimum offset has occurred across the eastern strand.

Leuhman Fault

The Leuhman Fault was first mapped by Dibblee (1960, 1967), who identified it as a down-on-the-northeast fault on the basis of tilted Tertiary sedimentary rocks and an elongate low area approximately 22 km northwest of Helendale, Calif. Dibblee (1960, 1967) inferred the concealed northwest-striking Leuhman Fault is near the eastern side of Mound (fig. 2) on the basis of the fault orientation where observed at its southeastern end. During our remote sensing analysis, we observed northwest-trending scarps in the pediment (Qpv) east of Leuhman Ridge near the inferred trace of the Leuhman Fault, but field observations demonstrated that these represent steps in the pediment surface and are not fault related. Moreover, measurements of depth to bedrock in wells drilled along the inferred trace of the Leuhman Fault (Cromwell and others, 2020), as well as a recent depth-to-bedrock model (Langenheim and others, 2019), show no substantial changes indicative of vertical displacement (Cromwell and others, 2020). A northwest-trending lineament through the pediment east of Leuhman Ridge, parallel to Moon Road, could be a fold in the underlying bedrock, or the edge of a bedrock slab buried by the overlying veneer, but additional observations are needed to characterize this feature more definitively. Although we find little to no convincing evidence for the existence of the Leuhman Fault, we show the location of its trace as mapped by Dibblee (1960, 1967) on our overview of the map area (fig. 2). However, it is not included in the database (Cyr and Miller, 2023).

Boron Gate Fault

The possible Boron Gate Fault, named for the first time in this study, strikes east-northeast between the railroad tracks and Boron Sanitary Landfill near the northern exposed limit of the Spring Fault horsetail splay (fig. 2). It was first identified in high-resolution topography and other remote-sensing imagery as a prominent lineament and topographic scarp (fig. 2). Field observations demonstrate that this lineament is defined by the termination of granitic bedrock (Kg and Kgdl) along a ragged approximately 5- to 12-m-high scarp. Despite these geomorphic indicators of a fault, we observed no fault rock in poor exposures of bedrock units Kg and Kgdl or faulted sediment (such as Qyae, Qyed, or Qies); however, the scarp appears to be dextrally offset by two strands of the Spring Fault. Measurements of depth to bedrock in wells (Cromwell and others, 2020) across the lineament show a 71-meter, down-to-the-northwest drop in bedrock elevation across a distance of just approximately 300 m, consistent with a down to the northwest fault. We collected a sample of sediment from an intermediate-age eolian sheet deposit (Qies) in apparent depositional contact with leucocratic granodiorite (Kgdl) at the southwestern extent of the Boron Gate Fault for luminescence geochronology (USGS-20-003; table 1). The sand-sheet deposit appears to be unaffected by the Boron Gate Fault, the last rupture of which must be older than the pIR–IRSL age of 25.7±1.2 ka for the Qies deposit (table 1; Mahan and others, 2021). We estimate that this is a Quaternary fault; however, the surface expression is not definitive and more precise characterization would require additional geomorphic, geochronologic, and subsurface data.

Arroyos Fault

The probable Arroyos Fault, named for the first time in this study, is a southwest-striking fault subparallel to the crest of Leuhman Ridge and perpendicular to the arroyos incised into the northwest side of the ridge (fig. 2). It was identified during field work as a down-to-the-northwest normal fault on the basis of aligned saddles of highly fractured bedrock exposed at the surface near its northeastern end. Reexamination of high-resolution topography and other remote sensing imagery identified a geomorphic lineament in bedrock outcrops along the steep northwest front of Leuhman Ridge. This lineament is elsewhere buried by younger Holocene mixed alluvial and eolian (Qyae) and eolian (Qyed) sediments. If the location of the fault shown on the geologic map is correct, the fault juxtaposes similar rock units along its entire length. No inferences about net offset are possible other than large offset is not likely. Additional field work in the deep arroyos would provide further constraints on the characteristics of this probable fault.

Mound Fault

The probable Mound Fault, named for the first time in this study, strikes approximately east along the southern side of Mound (fig. 2). It is defined by a zone of highly fractured bedrock and a saddle between smaller bedrock hills between Mound and the northeastern end of Leuhman Ridge. Close field examination also found three sites of fractured and mineralized Pleistocene alluvial and eolian sedimentary deposits (Qiae). Reconnaissance measurements of fractures in bedrock and Quaternary units show two dominant orientations: approximately 100° and approximately 325°. Additional field work is needed to better document the fractures, the geometry of this probable fault, and to determine whether and how it interacts with the Arroyos and Leuhman Faults. Similar rocks are exposed on both sides of the fault and offset is not possible to constrain.

Rich Fault

The possible Rich Fault, named for the first time in this study, crosses Rich Road and is subparallel to Leuhman Ridge (fig. 2). It was first identified in high-resolution topography and other remote-sensing data as a northeast-trending, low, linear ridge. The ridge has a sharp southeastern-facing boundary along its northeast extent, which may be a fault. A lineament with the same trend is present farther to the southwest. Field observations found fractured bedrock; however, intermediate-age eolian sheet deposits (Qie) and overlying young mixed alluvial and eolian deposits (Qyae) that drape the ridge are not deformed. We collected a sample of an intermediate-age mixed alluvial fan and eolian deposit (Qiae) underneath a young mixed alluvial fan and eolian deposit (Qyae4) from a natural exposure along Rich Road, approximately 3.5 km to the south, for pIR–IRSL geochronology. The exposure shows Qiae deposits below a depositional contact with young mixed alluvial fan and eolian deposits (Qyae4), which we estimate to be between approximately 9 and 14 ka based on soil characteristics and regional correlation (Miller and others, 2009). Analysis of that sample yielded a pIR–IRSL age of 38.9±2.9 ka (table 1; Mahan and others, 2021). Any surface ruptures on the possible Rich Fault are therefore older than late Pleistocene. Additional field observation and subsurface data collection would be needed to further constrain its characteristics.

Hydrologic Implications

The following section describes how, in general, the surficial geologic units, faults, and fault characteristics observed during the geologic mapping described in this report may affect groundwater hydrology in the map area. Although informed by recent geologic mapping (for example, Miller and others, 2020) and previous hydrologic characterization of similar surficial geologic units (for example, Mirrus and others, 2009; Nimmo and others, 2009a, b) in the region, this qualitative analysis is not a replacement for more quantitative well tests or hydrologic models.

Bedrock in the Leuhman Ridge map area is composed entirely of Mesozoic intrusive units that range from leucocratic granite to gabbro in composition. Much of the rock is coarse grained and forms grus, the exceptions being the leucocratic granite (Kgl) and gabbro (Kgb) endmembers of the suite. Grus as thick as 17 meters above hard granitic rock was noted in many well logs (Cromwell and others, 2020). As a result, it is possible that an upper interval of relatively more permeable weathered bedrock (for example, Dewandel and others, 2006; Ceccato and others, 2021) is present across large portions of the map area. Fractured rock, present near mapped fault zones and observed in road cuts at many locations in Leuhman Ridge, may also have substantial permeability (for example, Dewandel and others, 2006; Ceccato and others, 2021). Of the surficial map units we examined, most are either alluvial or eolian and range in grain size from sand to pebbles. These units probably are quite permeable (for example, Mirrus and others, 2009; Nimmo and others, 2009a, b). The exceptions are Pleistocene eolian units, which not only have silt and possibly clay as primary constituents, but also have significant soil development that includes clay, silt, and $CaCO_3$ that fills pores in the sediment. This material is probably much less permeable than other surficial units (for example, Mirrus and others, 2009; Nimmo and others, 2009a, b).

Faults also create secondary fractures in bedrock (for example, Caine and others, 1996; Evans and others, 1997; Zhang and Tullis, 1998). We did not find any complete exposures of fault cores or damage zones. However, the several kilometers of offset across the Spring Fault, inferred from displacement of units Kg and Kgd, indicates that there is likely a well-developed fracture zone in bedrock on both sides of the Spring Fault because fault zone widths and fracture densities are positively correlated with total offset (for example, Mitchell and Faulkner, 2009). Faults in the mapped area probably consist of damaged rock adjacent to a fault core (for example, Caine and others, 1996; Evans and others, 1997; Zhang and Tullis, 1998). Fractured rock adjacent to fault cores is generally permeable, although zones such as shear bands with mineralization and greater communition to fine grain size (cataclasite) may inhibit permeability (for example, Dorsey and others, 2021). In contrast, fault cores commonly form impediments to groundwater flow owing to very low permeability caused by several factors, including very fine grain size, mineralization, and lateral structural continuity of fine sheet-like structures. As a result, individual faults tend to behave both as conduits for enhanced lateral groundwater flow parallel to the fault in damaged rock adjacent to the fault core and as impediments to flow across the fault core. A network of faults, such as the five horsetail splays of the northern Spring Fault, may be especially effective as both impediments and lateral conduits.

On the basis of the topography of the map area, the geometry of faults observed during our geologic mapping, and the above discussion regarding the general hydrologic properties of the observed surficial units and previous work related to fault and fault zone permeability, we offer several hypotheses for groundwater flow that can be tested by more quantitative methods. Groundwater flow to the northwest, from the topographic high of Leuhman Ridge toward Rogers Lake,

could potentially be impeded by both the Arroyos and Rich Faults because these faults are nearly perpendicular to down-to-the-northwest topographic gradients and flow paths within presumed high-permeability materials (fig. 3; Tetra Tech, 2021). Hydraulic head differences across these faults would be positive tests for this hypothesis. Lateral flow along damage zones adjacent to the fault cores may result in flow to the southwest, parallel to the topographic gradient.

Groundwater flow to the east and northeast from Leuhman Ridge is toward the unnamed valley that lies west of the Kramer Hills and drains north toward Boron, Calif. (fig. 3; Tetra Tech, 2021). Available water-level data indicate that if the Leuhman Fault exists at depth, it may not impede groundwater flow (fig. 3; Tetra Tech, 2021); further study would be needed to demonstrate the possible effects of subsurface geology on groundwater flow.

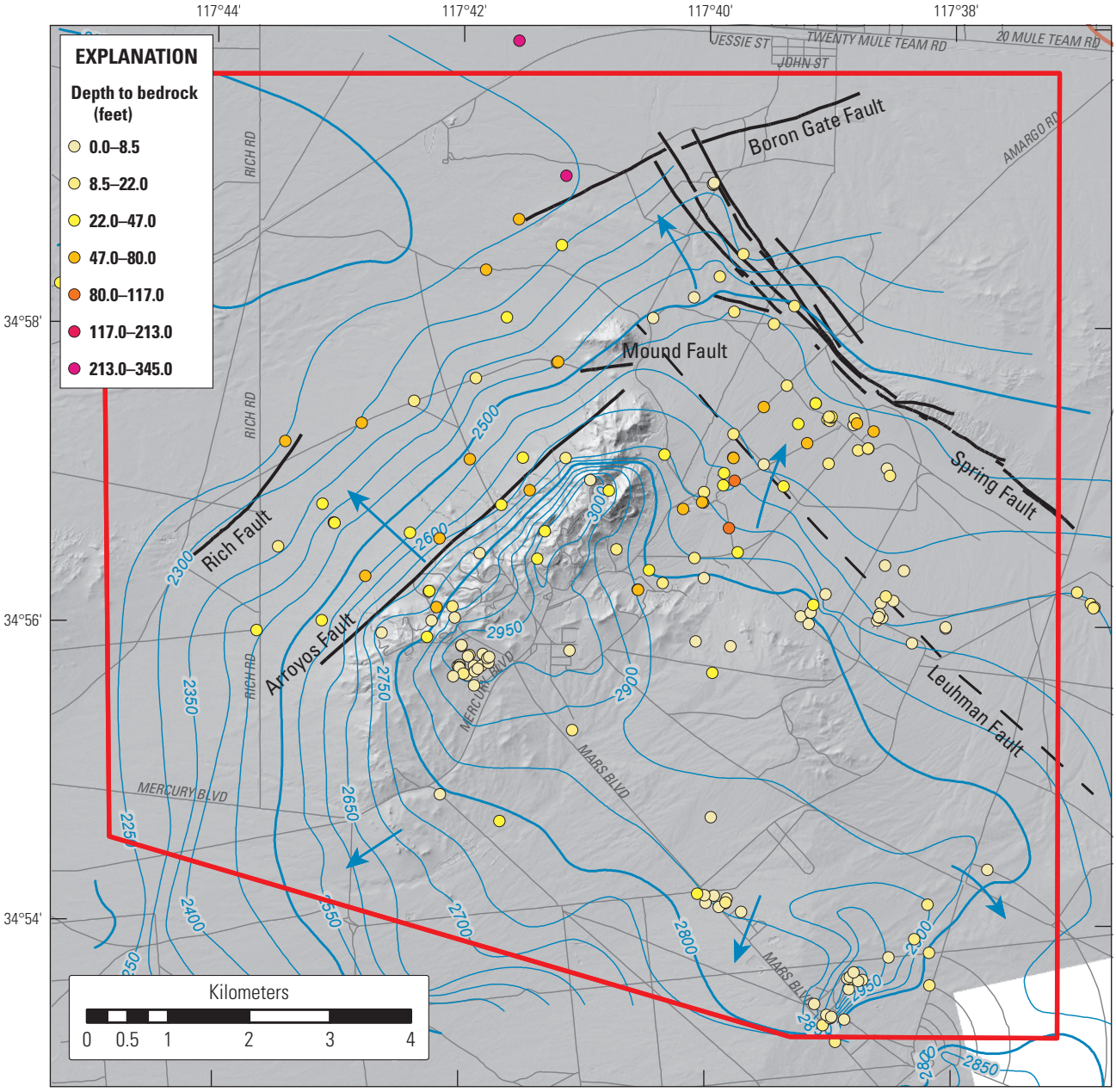

Figure 3. Map showing the depth to the top of bedrock (from Cromwell and others, 2020) and to the water table of part of the Air Force Research Laboratory (AFRL), northeast Edwards Air Force Base, California. Blue contours show elevation of groundwater table in feet (Tetra Tech, 2021) and arrows indicate general direction of groundwater flow; contour interval is 50 feet. Red polygon is area of surficial geologic map. Solid black lines are faults described in this report. Long dashed black line is projected trace of the Leuhman Fault (Dibblee, 1960). Base modified from U.S. Geological Survey, Leuhman Ridge, 2018, scale 1:24,000; and Kramer Junction, 2018, scale 1:24,000. Hillshade from U.S. Geological Survey digital elevation model data (U.S. Geological Survey, 2019).

Groundwater-discharge deposits (Qigw) observed in the horsetail splay of the Spring Fault indicate that this fault likely impeded shallow groundwater flow during the late Pleistocene; more recent groundwater flow could have been impeded by the horsetail splays of the Spring Fault (fig. 3). Flow could be directed northwestward along these northwest-striking faults, toward the Boron Gate Fault, however, additional data are necessary to confirm that the Spring Fault affects groundwater flow in the northeast part of the study area. Well data along the Boron Gate Fault are sparse (Cromwell and others, 2020), and additional data are needed to determine whether this structure, which offsets unweathered bedrock, impedes groundwater flow to the north and northwest. Additionally, if the Mound Fault possesses substantial east-west fracture zones (a possibility given our preliminary fracture analysis), it could act as a conduit for groundwater flow across the topographic saddle between Leuhman Ridge and Mound. Changes in the geometry and hydrologic properties of the Mound and Leuhman Faults since Pleistocene time, and whether and how those fault zones may be connected at depth, may be key to understanding groundwater flow across and beneath Leuhman Ridge.

Geologic Mapping Conventions

The geologic map is focused on description and interpretation of late Cenozoic deposits. In general, older rocks are crystalline and dense and have much less abundant and recoverable groundwater in comparison to younger and more porous Quaternary deposits, though this can be modified by fracture- and weathering-related secondary porosity and permeability. The older rocks vary considerably in age and composition; their material properties largely determine the properties of sediment eroded from them and therefore are classified by general groupings of age and composition.

Quaternary surficial deposits are mapped based on erosional or depositional process, and relative age classifications are based on characteristic soil development, geomorphic relations, and surficial characteristics, techniques developed by myriad researchers in arid and semi-arid regions and based primarily on the work of Bull (1991). The rates and magnitudes of these processes are functions of five main factors: climate, biologic activity, topography, parent (or initial) material, and time (Birkeland, 1999). As such, geomorphic surfaces with similar characteristics can be interpreted to have been deposited under grossly similar conditions and to have experienced similar postdeposition alterations. Depositional processes (overland flow, eolian transport, mass wasting) largely control the nature of the original deposit, which was governed by physical processes involving some aspect of topography. In many cases, particularly in tectonically inactive areas, climate is considered to be the dominant factor through time, and similar soils developed in deposits created by the same inferred depositional process can generally be considered contemporaneous; although variations, particularly lithologic, biologic, and climatic variations with elevation, can render deposits of the same age to have different soil-geomorphic characteristics. Because soil development is unidirectional—for example the relative thickness of the A horizon, the degree of reddening in B horizon, or the stage of pedogenic carbonate morphology only increase—relative differences in these properties can be used to classify Quaternary surficial deposits into a relative time scale. This concept has been demonstrated by numerous researchers in the Mojave Desert and Great basin (for example, Bedford, 2003; McDonald, 1994; Menges and others, 2001; Reheis and others, 1989; Wells and others, 1990; Yount and others, 1994).

Surficial geologic units commonly exist as veneers (<2 m) over older units. In areas where this relation is commonly observed, the underlying unit is stored in the "UnderMapUnit" field of the "MapUnitPoints" and "MapUnitPolys" feature classes of the database that accompanies this report (Cyr and Miller, 2023). Thus, a unit with Qyae in the "Symbol" field and Qie in the "UnderMapUnit" field, indicates an area where a veneer of young mixed alluvial fan and eolian deposits (Qyae) overlies intermediate-age eolian deposits (Qie). If the map is symbolized using the "Label" field then a slash (/) indicates this over/under relationship, with the younger, or overlying unit, indicated first. For example, Qyae/Qie.

The areal extent of individual deposits is commonly so small that each deposit cannot be shown individually at map scale. Areas consisting of deposits too small to show individually within a larger polygon representing a different unit, but that represent more than 20 percent of the area of the larger polygon, are stored in the "SubordinateMapUnit" field of the "MapUnitPoints" and "MapUnitPolys" feature classes of the database. Thus, a unit with Qies in the "Symbol" field and Qyae in the "SubordinateMapUnit" field, indicates an area with both Qies and Qyae deposits and associated surfaces, and unit Qies is more common than unit Qyae; other deposits may be present in the polygon but are less than 20 percent of the area of the mapped polygon. If the map is symbolized using the "Label" field then a plus (+) indicates this dominant+subordinate relationship, with the more common unit indicated first. For example, Qies+Qyae.

DESCRIPTION OF MAP UNITS

[Soil Av and B horizon descriptions follow Birkeland (1999). Carbonate stage morphology (for example, Stage I, Stage III$^+$) follows Gile and others (1966), modified by Machette (1985). pIR–IRSL, post-infrared–infrared stimulated luminescence; CI, color index]

SURFICIAL DEPOSITS

ANTHROPOGENIC DEPOSITS

ml **Modified land (latest Holocene)**—Material moved for construction purposes and agricultural disturbances sufficiently extensive to make landforms and deposits difficult to identify

WASH DEPOSITS

Qaw **Active wash deposits (latest Holocene)**—Alluvial deposits of confined streams characterized by surfaces and channels actively receiving sediment in the last few decades. Loose, poorly to moderately sorted, fine- to very coarse grained sand and pebble to cobble sediment. Evidence for recent to modern surface-water flow, such as reduced perennial vegetation, significant bar and swale topography, and lack of soil development. Mapped mainly where ephemeral stream flow is channelized. Bar and swale topography pronounced along longer streams, such as along southern side of Kramer Hills, and in systems with bimodal sand-gravel grain-size distributions. Equivalent to Qya1 and Qya2 alluvial fan units of Miller and others (2009)

Qyw **Young wash deposits (latest Pleistocene to Holocene)**—Largely inactive alluvial wash deposits either in terraces adjacent to active wash surfaces or in shallow swales on young alluvial fan deposits (Qya). Loose to weakly compacted, poorly to moderately sorted, fine- to very coarse grained sand and pebble sediment. No evidence for recent surface-water flow. Soil development typically expressed as 1- to 2-cm-thick, incipient to weak, silty fine-grained sand A horizon above a weak cambic B horizon (Bw). Moderate remnant depositional bar and swale topography, with relief between approximately 10 and 30 cm

ALLUVIAL FAN DEPOSITS

Qya **Young alluvial fan deposits (latest Pleistocene to Holocene)**—Alluvial fan deposits characterized by surfaces that are abandoned or receive flood sediments on a centennial to millennial basis. Poorly to moderately sorted, loose to weakly compacted gravel and sandy gravel. No to very weak desert pavement with no to incipient varnish on individual clasts. Soil development typically expressed as 1- to 3-cm-thick, incipient to weak, very fine to fine-grained sandy silt Av above a weak Bw. Moderate to weak remnant depositional bar and swale topography, with relief between approximately 10 and ~40 cm. Deposits restricted to eastern side of Leuhman Ridge, where less eolian sediment is present. As mapped, includes narrow active washes too small to depict on map. Locally divided into the following subunit:

Qya4 **Older young alluvial fan deposits (latest Pleistocene to earliest Holocene)**—Characterized by surfaces abandoned for approximately 9,000 to 14,000 years. Poorly to moderately sorted gravel to sandy gravel and gravelly sand; sediments light to dark gray to brown, slightly compacted to lightly cemented. Surfaces show significant post-depositional modification, including weak remnant depositional bar and swale topography with relief defined by the grain size of coarser clasts in the remnant bars. Generally better sorting of clasts across the surface, with weak to moderate development of desert pavement and weak to moderate varnish. Soil development expressed as weak to moderately developed Av, typically 3 to 5 cm thick, composed of loose silt and fine-grained sand, with an incipient to weakly developed Bw horizon, slight reddening of undersides of surface clasts, and Stage I to I$^+$ soil carbonate development. Moderately to well vegetated by *Larrea tridentata* (creosote bush) and *Ambrosia dumosa* shrubs

Qyag **Young alluvial fan deposits composed primarily of grus (latest Pleistocene to Holocene)**—Alluvial fan deposits composed primarily of clasts from granitic source that weathers to grus, characterized by surfaces that are abandoned or receive flood sediments on a centennial to millennial basis. Moderately to well-sorted, loose to weakly compacted very coarse sand to pebbly sand. Generally, no desert pavement or varnish on surface clasts, though it may occur locally depending on grain size and lithology. Soil development typically expressed as 2- to 3-cm-thick, weak, fine-grained sandy silt Av above a weak to moderately reddened Bw. Surfaces are most common downslope of Cretaceous granite outcrops. Extent limited to saddle between Mound and northeastern end of Leuhman Ridge and to northeastern side of Leuhman Ridge and northern edge of adjacent pediment

Qia **Intermediate-age alluvial fan deposits (middle to late Pleistocene)**—Alluvial fan deposits characterized by surfaces abandoned for tens of thousands of years. Poorly to moderately sorted, compacted, pebble to coarse-cobble sandy gravel. Surfaces characterized by moderately to well-developed desert pavement with moderate to strong varnish on clasts. Soil development typically expressed as 4- to 6-cm-thick silt to clayey silt Av, strong Bw, and moderate to strongly developed translocated clay in lower part of B horizon (Bt). Stage II^+ to III^+ calcic horizon. No remnant depositional topography. Pavement may be degraded along edges of convergent zones where younger flow of water across surface is beginning to dissect surface

Qiag **Intermediate-age alluvial fan deposits composed primarily of grus (middle to late Pleistocene)**—Alluvial fan deposits composed primarily of clasts from granitic source that weathers to grus, characterized by surfaces abandoned for tens of thousands of years. Moderately to well-sorted, moderately compacted, pebbly coarse sand. Moderately developed desert pavement with no to weak varnish of clasts. Soil development typically expressed as 3- to 4-cm-thick sandy silt Av, moderately developed Bw, and Stage I^+ to II^- pedogenic carbonate, comprising discontinuous rinds on coarser clasts and small (<1 cm) carbonate nodules in very coarse grained sand to granular matrix. Surfaces most commonly overlying or adjacent to outcrops of Cretaceous granite pediments (Qpv). Only observed as an underlying unit to younger deposits in the map area

EOLIAN DEPOSITS

Qyed **Young eolian dune deposits (latest Pleistocene to Holocene)**—Eolian sand deposits that form dunes. Commonly steep-sided and composed of moderately to well-bedded fine- to medium-grained sand; generally stabilized by creosote bush, *Senegalia greggii* (catclaw acacia), and *Ambrosia dumosa* shrubs, and annual grasses. Weak to no soil development, typically expressed as 1- to 2-cm-thick silty sand A horizon over an incipient to weak Bw. Primarily observed between Leuhman Ridge and eastern side of Rogers Dry Lake bed; deposits both linear and parabolic in form. Climbing and falling dunes (sand ramps) are also mapped primarily along western side of Leuhman Ridge. Sample of Qyed sediment (USGS-20-001) collected from side of an arroyo draining west side of Leuhman Ridge yielded a pIR–IRSL age of 8.32±0.71 ka (table 1)

Qyes **Young eolian sand-sheet deposits (latest Pleistocene to Holocene)**—Loose to moderately compacted, well-sorted, horizontally laminated to structureless sand-sheet deposits generally forming a subhorizontal surface over older eolian deposits

Qie **Intermediate-age eolian deposits (middle to late Pleistocene)**—Eolian sand deposits inactive for tens of thousands of years. Moderately to well-compacted, well-sorted, medium-grained sand. Strong soil development, with upper part of profile absent. Soil typically exhibited as strong Bt with Stage III to IV^- carbonate as platy horizons and platy, vertical bands precipitated in soil fractures. Underlies younger deposits in much of area north and west of Leuhman Ridge. Where exposed at surface it has a 2- to 4-cm-thick sandy, clayey silt Av horizon over a strong, dark-red Bw. Stage III to IV^- soil carbonate commonly present within 20 to 30 cm of ground surface. Surface may show decimeter-diameter polygonal fracture pattern. Characterized by presence of annual grasses and *Atriplex* sp. (salt bush), and by lack of creosote bush. Subdivided into sand-sheet deposits. Can be subdivided into Qied, defined as deposits that have similar depositional characteristics and landscape position to Qyed but similar stratigraphic position and pedogenic characteristics to Qies. Where observed in subvertical outcrop exposed in deep arroyos, Qie and Qied deposits are buried beneath several meters of Qyed or Qyae deposits and so are not depicted on map. Sample of Qied sediment (USGS-20-002) collected from side of an arroyo draining west side of Leuhman Ridge yielded a pIR–IRSL age of 15.2±0.7 ka (table 1)

Qies **Intermediate-age eolian sheet deposits (middle to late Pleistocene)**—Eolian sand-sheet deposits inactive for tens of thousands of years. Moderately to well-compacted, well-sorted, medium-grained sand. Strong soil development, with upper part of profile absent. Soil typically exhibited as strong Bt with Stage III to IV- carbonate as platy horizons and platy, vertical bands precipitated in soil fractures. Underlies younger deposits in much of area north and west of Leuhman Ridge. Where it is exposed at surface it has a 2- to 4-cm-thick sandy clayey silt Av horizon over a strong, dark red Bw. Stage III to IV^- soil carbonate commonly present within 20 to 30 cm of ground surface. Surface may show decimeter diameter polygonal fracture pattern. Characterized by presence of annual grasses and salt bush, and lack of creosote bush. Sample of Qies (USGS-20-003) collected where it overlies Kgdl between splays of the Spring Fault yielded a pIR–IRSL age of 25.7±1.2 ka (table 1)

PLAYA DEPOSITS

Qyp **Young playa deposits (latest Pleistocene to Holocene)**—Playa deposits that are rarely flooded. Composed of moderately to well-sorted, compacted silt, clay, and sand. Generally flat to undulating and lacking vegetation

MIXED ALLUVIAL FAN AND EOLIAN DEPOSITS

Qyae **Young mixed alluvial fan and eolian sand deposits (latest Pleistocene to Holocene)**—Alluvial fan and eolian sediments that are thoroughly mixed, with alluvial process dominant. Loose to slightly compacted, gravelly sand with vague to well-defined, thin bedding. Forms flatter surfaces than temporally equivalent unit with lack of eolian sand, Qya, because eolian sand additions mute topography. Weak to no soil development typically expressed as a thin sandy silt A horizon over an incipient to weak Bw horizon. Sparsely to moderately vegetated, generally supporting creosote bush. Sample of Qyae sediment (USGS-20-001) collected from near contact with Klg on west side of Leuhman Ridge yielded a pIR–IRSL age of 8.32±0.71 ka (table 1). May include narrow stream channels, difficult to distinguish and map separately. Locally divided into the following subunit:

Qyae4 **Older young mixed alluvial fan and eolian sand deposits (latest Pleistocene to earliest Holocene)**—Alluvial-fan and eolian sediments that are thoroughly mixed, with alluvial processes dominant. Characterized by surfaces abandoned for approximately 9,000 to 14,000 years. Moderately sorted, loose to slightly compacted gravelly sand with vague to well-defined, thin bedding. Forms flatter surfaces than temporally equivalent unit Qya4 that lacks eolian sand, because eolian sand additions mute topography. Soil development expressed as weak to moderately developed Av, typically 3 to 5 cm thick, composed of loose silt and fine-grained sand, with a weakly developed Bw horizon, slight reddening of undersides of surface clasts, and Stage I to I^+ soil carbonate development. Moderately to well vegetated by creosote bush and *Ambrosia dumosa* shrubs

Qiae **Intermediate-age mixed alluvial fan and eolian sand deposits (middle to late Pleistocene)**—Alluvial fan and eolian sand sediments that are thoroughly mixed, with alluvial processes dominant. Moderately compact gravelly sand deposits with generally flat surfaces, inconsistently developed desert pavement, Bw, Bt, and pedogenic carbonate. Sparse vegetation, primarily creosote bush. Sample of Qiae sediment (USGS-20-004) collected from road cut at southern end of Rich Road yielded a pIR–IRSL age of 38.9±2.9 ka (table 1)

GROUNDWATER-DISCHARGE DEPOSITS

Qigw **Intermediate-age groundwater-discharge deposits (middle to late Pleistocene)**—Reddish-brown, muddy, fine- to medium-grained sand with abundant white nodules, plates, and "popcorn" masses of $CaCO_3$. Grades laterally into Qiae deposits with very common carbonate nodules. Primarily mapped east of Mound. Represents wetland deposits

EROSIONAL SURFACES

PEDIMENT SURFACES

[Gently-sloping erosional surfaces in various stages of erosion and burial. Generally forms in felsic granite that weathers to grus]

Qpv **Veneered pediment (Quaternary)**—Gently sloping erosion surface in various stages of erosion and burial. Generally forms in felsic granite that weathers to grus. Fairly smooth veneer of sediment, commonly alluvial in nature, generally less than 2 m thick on pediment surface; soil development variable with age of sediment. Mapped where bedrock is exposed in small knobs, road cuts, or washes

SUBSTRATE MATERIALS (PRE-QUATERNARY)

Klg **Leucocratic granite (Cretaceous)**—Generally fine-grained, silicic, white biotite granite. Underlies much of Leuhman Ridge. Highly variable rock texture and composition, with grain size ranging from very fine to medium and CI ranging from 2 to 8%. Many exposures consist of generally fine-grained and very leucocratic complexly anastomosing dikes that may represent one or more dike swarms. Many dikes are seriate, with quartz and feldspar ranging from very fine to fine grained with a few grains as coarse as medium. Patches of medium-grained rock, possibly host to dikes, are biotite granite similar to unit Kg. Most exposures display complex fracturing and alteration

Kg **Granite (Cretaceous)**—Light-gray biotite granite, generally underlying broad, undulating pediment topography. Medium- to coarse-grained granite with CI ranging from 6 to 15%. Equigranular to sparsely porphyritic. Intruded by dikes of aplite, quartz-rich pegmatite, and pegmatite. Unfoliated, although in a few places a shape-preferred orientation of biotite defines a magmatic foliation. Grades to unit Klg in a zone of increasing dikes over a width of a few tens of meters

Kgd **Granodiorite (Cretaceous)**—Gray hornblende-biotite granodiorite forming an elongate body east of Spring Fault and present in smaller bodies farther west. Coarse grained with hornblende as large as 3×0.5 cm; CI ranging from 15 to 25%. Strongly foliated. Includes enclaves of fine-grained mafic rock and bodies of gabbro from 2 m to tens of meters wide (unit Kgb). Intruded by dikes of aplite, pegmatite, and quartz-rich pegmatite, as well as granite of unit Kg. Appears to grade laterally into leucocratic granodiorite (unit Kgdl) with decrease of mafic minerals and increase of quartz

Kgdl **Leucocratic granodiorite (Cretaceous)**—Light-gray biotite to biotite-hornblende granodiorite exposed in northeastern flank of Mound and areas to the northeast. Coarse grained and strongly foliated; CI ranging from 4 to 12%. Spatially associated with units Kgb and Kgd

Kgb **Gabbro (Cretaceous)**—Dark-gray hornblende gabbro that forms small bodies in units Kgd and Kgdl and larger bodies in a few places east of Mound. Very coarse grained with 50% hornblende to medium-coarse grained with approximately 30% hornblende and approximately 10% biotite. Strongly foliated. Cut by leucocratic dikes with commonly gradational margins

Kpgd **Porphyritic granodiorite (Cretaceous)**—Sparsely porphyritic biotite granodiorite with local hornblende. Strongly foliated with quartz and biotite forming grain-dimensional fabric. Limited in extent; observed only near southwestern mapped extent of young eolian dune deposits (Qyed) at western edge of map area

References Cited

Bedford, D.R., 2003, Surficial and bedrock geologic map database of the Kelso 7.5-Minute quadrangle, San Bernardino County, California: U.S. Geological Survey Open-File Report 03–501, scale 1:24,000, 34 p. [Available at http://geopubs.wr.usgs.gov/open-file/of03-501/].

Birkeland, P.W., 1999, Soils and geomorphology: New York, Oxford University Press, 430 p.

Caine, J.S., Evans, J.P., and Forster, C.B., 1996, Fault zone architecture and permeability structure: Geology, v. 24, p. 1025–1028.

Bull, W.B., 1991, Geomorphic responses to climate change: New York, Oxford University Press, 326 p.

Ceccato, A., Vioa, G., Tartaglia, G., and Antonellini, M., 2021, In-situ quantification of mechanical and permeability properties on outcrop analogues of offshore fractured and weathered crystalline basement—Examples from the Rolvsnes granodiorite, Bømlo, Norway: Marine and Petroleum Geology, v. 124, 104859, https://doi.org/10.1016/j.marpetgeo.2020.104859.

Cromwell, G., Fenton, N.C., and Ely, C.P., 2020, Select borehole data for Edwards Air Force Base and vicinity, Antelope Valley, CA: U.S. Geological Survey data release, https://doi.org/10.5066/P90N3MQQ.

Cyr, A.J., and Miller, D.M., 2023, Digital database for the preliminary surficial geologic map of Leuhman Ridge and the surrounding area, Edwards Air Force Base and Air Force Research Laboratory, Kern and San Bernardino Counties, California: U.S. Geological Survey data release, https://doi.org/10.5066/P9WTKPBP.

Dewandel, B., Lachassange, P., Wyns, R., Maréchal, J.C., Krishnamurthy, N.S., 2006, A generalized 3-D geological and hydrogeological conceptual model of granite aquifers controlled by single or multiphase weathering: Journal of Hydrology, v. 330, p. 260–284.

Dibblee, T.W., 1960, Geology of the Rogers Lake and Kramer quadrangles, California: U.S. Geological Survey Bulletin 1089-B, scale 1:62,500.

Dibblee, T.W., 1967, Areal geology of the western Mojave Desert, California: U.S. Geological Survey Professional Paper 522, 153 p.

Dokka, R.K., and Travis, C.J., 1990, Role of the eastern California shear zone in accommodating Pacific-North American plate motion: Geophysical Research Letters, v. 17, p. 1323–1226.

Dorsey, M.T., Rockwell, T.K., Girty, G.H., Ostermeijer, G.A., Browning, J., Mitchell, T.M., Fletcher, J.M., 2021, Evidence of hydrothermal fluid circulation driving elemental mass redistribution in an active fault zone: Journal of Structural Geology, v. 144, https://doi.org/10.1016/j.jsg.2020.104269.

Durcan, J.A., King, G.E., and Duller, G.A.T., 2015, DRAC—Dose rate and age calculator for trapped charge dating: Quaternary Geochronology, v. 28, p. 54–61.

Evans, J.P., Forster, C.B., Goddard, J.V., 1997, Permeability of fault-related rocks and implications for hydraulic structure of fault zones: Journal of Structural Geology, v. 19, p. 1393–1404. https://doi.org/10.1016/S0191-8141(97)00057-6.

Gile, L.H., Perterson, F.F., and Grossman, R.B., 1966, Morphological and genetic sequences of carbonate accumulations in desert soils: Soil Science, v. 101, no. 5, p. 347–360.

Kreutzer, S., Schmidt, C., Fuchs, M.C., Dietze, M., Fischer, M., Fuchs, M., 2012, Introducing an R package for luminescence dating analysis: Ancient TL, v. 30, no. 1, 8 p.

Langenheim, V.E., Morita, A., Christensen, A.H., Cromwell, G., and Ely, C., 2019, Depth to bedrock based on modeling of gravity data of the eastern part of Edwards Air Force Base, California: U.S. Geological Survey Open-File Report 2019–1128, 12 p., https://doi.org/10.3133/ofr20191128.

Machette, M.N., 1985, Calcic soils of the southwestern United States, *in* Weide, D.L., ed., Soils and Quaternary geology of the southwestern United States: Geological Society of America Special Paper 203, 21 p.

Mahan, S.A., Gray, H.J., Cyr, A.J., Krolczyk, E.T., and Miller, D.M., 2021, Data release for luminescence—Edwards Air Force Base (CA) and CA Water Science Center report including luminescence data and ages: U.S. Geological Survey data release, https://doi.org/10.5066/P9IXG2JX.

McDonald, E.V., 1994, The relative influences of climatic change, desert dust, and lithologic control on soil-geomorphic processes and soil hydrology of calcic soils formed on Quaternary alluvial-fan deposits in the Mojave Desert, California: Albuquerque, University of New Mexico, Ph.D. Dissertation, 382 p.

Menges, C.M., Taylor, E.M., Workman, J.B., and Jayko, A.S., 2001, Regional surficial-deposit mapping in the Death Valley area of California and Nevada in support of ground-water modeling, *in* Machette, M.N., Johnson, M., and Slate, J.L., eds., Quaternary and late Pliocene geology of the Death Valley region—Recent observations on tectonics, stratigraphy, and lake cycles: U.S. Geological Survey Open-File Report 01–0051, p. 151–166.

Miller, D.M., and Yount, J.L., 2002, Late Cenozoic tectonic evolution of the north-central Mojave Desert inferred from fault history and physiographic evolution of the Fort Irwin area, California: Geological Society of America Memoir, v. 195, p. 173–197.

Miller, D.M., Bedford, D.R., Hughson, D.L., McDonald, E.V., Robinson, S.E., and Schmidt, K.M., 2009, Mapping Mojave Desert Ecosystem properties with Surficial Geology, *in* Webb, R.H., Fenstermaker, L.F., Heaton, J.S., Hughson, D.L., McDonald, E.V., Miller, D.M., eds.., The Mojave Desert—Ecosystem processes and sustainability: Reno, Nev., University of Nevada Press, p. 225–251.

Miller, D.M., Langenheim, V.E., and Haddon, E.K., 2020, Geologic map and borehole stratigraphy of Hinkley Valley and vicinity, San Bernardino County, California: U.S. Geological Survey Scientific Investigations Map 3458, pamphlet 23 p., 2 sheets, scale 1:24,000, https://doi.org/10.3133/sim3458.

Mirrus, B.B., Perkins, K.S., Nimmo, J.R., and Singha, K., 2009, Hydrologic characterization of desert soils with varying degrees of pedogenesis—2. Inverse modeling for effective properties: Vadose Zone Journal, v. 8, p. 496–509.

Mitchell, T.M., and Faulkner, 2009, The nature and origin of off-fault damage surrounding strike-slip fault zones with a wide range of displacements—A field study from the Atacama fault system, northern Chile: Journal of Structural Geology, v. 31, p. 802–816.

Nimmo, J.R., Perkins, K.S., Schmidt, K., Miller, D.M., Stock, J.D., and Singha, K., 2009a, Hydrologic characterization of desert soils with varying degrees of pedogenesis—1. field experiments evaluating plant-relevant soil water behavior: Vadose Zone Journal, v. 8, p. 480–495.

Nimmo, J.R., Schmidt, K.M., Perkins, K.S., and Stock, J.D., 2009b, Rapid measurement of field-saturated hydraulic conductivity for areal characterization: Vadose Zone Journal, v. 8, p. 142–149.

Nuriel, P., Miller, D.M., Schmidt, K.M., Coble, M.A., Maher, K., 2019, Ten-million years of activity within the Eastern California Shear Zone from U-Pb dating of fault-zone opal: Earth and Planetary Science Letters, v. 521, p. 37–45, https://doi.org/10.1016/j.epsl.2019.05.047.

Orme, A.R., 2008, Lake Thompson, Mojave Desert, California—The late Pleistocene lake system and its Holocene desiccation, *in* Reheis, M.C., Hershler, R., and Miller, D.M., eds., Late Cenozoic drainage history of the southwestern Great Basin and Lower Colorado River region—Geologic and Biotic Perspectives: Geological Society of America Special Paper 439, p. 261–278.

Reheis, M.C., Harden, J.W., McFadden, L.D., and Shroba, R.R., 1989, Development rates of late Quaternary soils, Silver Lake playa, California: Soil Science Society of America Journal, v. 53, no. 4, p. 1127–1140.

Tetra Tech Groundwater, 2021 groundwater monitoring report, northeast Air Force Research Laboratory groundwater area, Operable unit 4/9, Edwards Air Force Base, California: California Water Resources Control Board, 2,458 p. [Available at https://documents.geotracker.waterboards.ca.gov/esi/uploads/geo_report/2200948894/DOD100111600.PDF]

U.S. Geological Survey [USGS], 2019, 3D Elevation Program 1-meter resolution Digital Elevation Model [Elevation Products 3DEP, 1 meter DEM, CA SoCal Wildfires B2 2018]: U.S. Geological Survey web page, accessed March 10, 2020, at https://apps.nationalmap.gov/downloader/.

U.S. Geological Survey and California Geological Survey, 2019, Quaternary fault and fold database for the United States: U.S. Geological Survey database, accessed October 1, 2021, at https://www.usgs.gov/programs/earthquake-hazards/faults.

U.S. Geological Survey National Geospatial Technical Operations Center, 2022, USGS National Transportation Dataset (NTD) for California (published 20221115) FileGDB: U.S. Geological Survey data release. [Available at https://www.sciencebase.gov/catalog/item/5f6345c082ce38aaa238c9a3]

Ward, A.W., and Dixon, G.L., 2002a, Preliminary geologic map of the Rogers Lake North Quadrangle, Kern County, California: U.S. Geological Survey Open-File Report 93-694, scale 1:24,000.

Ward, A.W., and Dixon, G.L., 2002b, Preliminary geologic map of the Rogers Lake South Quadrangle, Los Angeles and Kern Counties, California: U.S. Geological Survey Open-File Report 93-696, scale 1:24,000.

Wells, S.G., McFadden, L.D., and Harden, J., 1990, Preliminary results of age estimations and regional correlation of Quaternary alluvial fans within the Mojave Desert of southern California, *in* Reynolds, R.E., Wells, S.G., Brady, R.H., III, and Reynolds, J., eds., At the end of the Mojave—Quaternary studies in the eastern Mojave Desert: San Bernardino County Museum Association Special Publication, p. 45–53.

Yount, J.C., Schermer, E.R., Felger, T.J., Miller, D.M., and Stephens, K.A., 1994, Preliminary geologic map of Fort Irwin basin, north-central Mojave Desert, California: U.S. Geological Survey Open-File Report 94–173, scale 1:24,000, 27 p.

Zhang, S., and Tullis, T.E., 1998, The effect of fault slip on permeability and permeability anisotropy in quartz gouge: Tectonophysics, v. 295, p. 41–52.

Glossary

approximately located Location generally is accurate within 15 m of where feature is plotted on the map.

certain Existence and identity can be determined using relevant observations and scientific judgement; therefore, one can be confident in the credibility of this interpretation. When used for the location of a feature, location is accurately plotted within 5 meters of where it is plotted on the map.

concealed A feature is not observable because it is completely concealed by an overlying map unit or a body of water or ice, although it may be observable nearby. By definition its plotted position on the map may not be within the declared zone of confidence.

fault A surface or zone along which there has been sensible displacement, or the observed or inferred trace of such a surface or zone on the landscape. May or may not separate map units.

gradational A gradual or continuous lithologic or compositional change from one geologic map unit to another.

inferred A feature that is not directly observable, so its identity and location must be inferred by indirect means. By definition its plotted position on the map may not be within the declared zone of confidence.

lineament A linear surface feature of unspecified, and perhaps unknown, origin. Commonly observed via aerial photographs or inspection of topography.

probable Existence or identity can be determined using relevant observations and scientific judgement, but additional observations are needed to be certain.

possible Existence or identity is consistent with the relevant observations and scientific judgement, but direct observations are absent or ambiguous.